Journal of Chromatography A, 1218 (2011) 4149–4159

Contents lists available at ScienceDirect

Journal of Chromatography A

journal homepage: www.elsevier.com/locate/chroma

Dissolution and nanoparticle generation behavior of Be-associated materials in synthetic lung fluid using inductively coupled plasma mass spectroscopy and flow field-flow fractionation

Wenjie Huang[a,b], Diego Fernandez[a], Abigail Rudd[a], William P. Johnson[a,*], David Deubner[c], Philip Sabey[c], Jason Storrs[d], Rod Larsen[d]

[a] Department of Geology and Geophysics, University of Utah, 135 South 1460 East, Salt Lake City, UT 84112, USA
[b] Department of Chemical Engineering, University of Utah, Salt Lake City, UT 84112, USA
[c] Brush Wellman Inc., Mayfield Heights, OH 44124, USA
[d] Rocky Mountain Center for Occupational Health and Safety, Salt Lake City, UT 84112, USA

ARTICLE INFO

Article history:
Available online 4 December 2010

Keywords:
Beryllium
Toxicity
Field flow fractionation
Nanoparticle
Particle
Dissolution

ABSTRACT

Various Be-containing micro-particle suspensions were equilibrated with simulated lung fluid (SLF) to examine their dissolution behavior as well as the potential generation of nanoparticles. The motivation for this study was to explore the relationship between dissolution/particle generation behaviors of Be-containing materials relevant to Be-ore processing, and their epidemiologically indicated inhalation toxicities. Limited data suggest that BeO is associated with higher rates of beryllium sensitization (BS) and chronic beryllium disease (CBD) relative to the other five relevant materials studied: bertrandite-containing ore, beryl-containing ore, frit (a processing intermediate), $Be(OH)_2$ (a processing intermediate), and silica (control). These materials were equilibrated with SLF at two pH values (4.5 and 7.2) to reflect inter- and intra-cellular environments in lung tissue. Concentrations of Be, Al, and Si in SLF increased linearly during the first 20 days of equilibration, and then rose slowly, or in some cases reached a maximum, and subsequently decreased. Relative to the other materials, BeO produced relatively low Be concentration in solution at pH 7.2; and relatively high Be concentration in solution at pH 4.5 during the first 20 days of equilibration. For both pH values, however, the Be concentration in SLF normalized to Be content of the material was lowest for BeO, demonstrating that BeO was distinct among the four other Be-containing materials in terms of its persistence as a source of Be to the SLF solution. Following 149 days of equilibration, the SLF solutions were fractionated using flow-field flow fractionation (FlFFF) with detection via ICP-MS. For all materials, nanoparticles (which were formed during equilibration) were dominantly distributed in the 10–100 nm size range. Notably, BeO produced the least nanoparticle-associated Be mass (other than silica) at both pH values. Furthermore, BeO produced the highest Be concentrations in the size range corresponding to < 3 kDa (determined via centrifugal ultrafiltration), indicating that in addition to persistence, the BeO produced the highest concentrations of truly dissolved (potentially ionic) Be relative to the other materials. Mass balance analysis showed reasonable sample recoveries during FFF fractionation (50–100%), whereas recoveries during ICP-MS (relative to acidified standards) were much lower (5–10%), likely due to inefficiencies in nebulizing and ionizing the nanoparticles.

1. Introduction

Occupational exposure limits for airborne beryllium (Be) adopted by OSHA address both acute beryllium disease and chronic beryllium disease (CBD). However, there is doubt as to the effectiveness of the current OSHA standard of 2 $\mu g/m^3$ 8-h time-weighted average in preventing CBD [1,2]. The specific mechanism leading to CBD is not known; one hypothesis is that CBD is driven by dissolution of Be from retained inhaled particles in contact with lung fluid, either providing continuously dissolved Be or being ingested by lung macrophages, which in turn drives the immune response, granulomatous inflammation, and fibrosis.

CBD incidences differ among different facilities, possibly due to differences in dissolution behaviors among their process materials

* Corresponding author. Tel.: +1 801 664 8289.
E-mail address: william.johnson@utah.edu (W.P. Johnson).

0021-9673/$ – see front matter © 2010 Elsevier B.V. All rights reserved.
doi:10.1016/j.chroma.2010.11.070

[3]. For a particular company with multiple Be processing facilities, incidence rates were higher for those facilities processing or generating BeO relative to a facility processing materials such as beryl and bertrandite (Supporting information, SI). The above observations suggest that differences in properties (e.g. recalcitrance to dissolution or propensity to generated other particles upon dissolution) among different ores may correspond to the relative incidences of CBD among the ores.

Airborne particles, particularly those particles in the <2.5 μm in diameter ($PM_{2.5}$), are found to be of great biological concern [4–10]. The toxicology of respiratory fine particle ($PM_{2.5}$) may be associated with the formation of nano-size particles in the lung fluid, and the accelerated dissolution–translocation relationships of these nano-sized particles [11]. The possible retention, or even generation, of nano- to micro-particles is a subject of growing interest due, for example, to the increased dispersion of engineered nano-sized particles (NP) in the environment, and the unknown biological impacts from these NP [12,13].

Among the techniques available to characterize size of nano- and micro-particles suspended in solution, is flow-field flow fractionation (FlFFF). The size fractionation of particles by FlFFF is typically carried out in an elongated, ribbon-like channel in which parabolic laminar carrier flow (channel flow) carries the particles to the channel exit and a detector [14–16]. A perpendicular cross-flow (through a membrane bounding one surface of the chamber) forces the particles toward the bounding membrane to an extent governed by back-diffusion of the particles (drag and diffusion forces depending independently on size). The particles become aligned within different streamlines in the laminar parabolic flow field according to their hydrodynamic size, resulting in their differential elution from the channel [15,17].

Flow field-flow fractionation (FlFFF) is a prominent technique for nanomaterial fractionation because of its excellent resolution and applicability to a wide range of sizes, particularly the ability to fractionate and characterize particles ranging in size from 3 nm to 200 nm [15,18–20]. This method has been greatly improved to yield lesser dilution by use of a trapezoid-shaped channel [21–23] in so-called asymmetric FlFFF, or AF4.

FlFFF coupled to inductively coupled plasma mass spectrometry (FFF-ICP-MS) is a powerful technique for characterization of nanomaterials, because it combines the rapid and non-invasive size fractionation analysis offered by FlFFF with the high-resolution and large dynamic range for elemental analyses provided by ICP-MS. The ability to simultaneously measure a wide range of elements allows FFF-ICP-MS to determine composition and compositional changes among size distribution fractions of nanomaterials, as has been proven for environmental colloids [24–28]. FFF-ICP-MS has been used successfully as well to examine the interaction of natural nanocolloids with trace elements [25,27,29].

Relative to chromatographic methods employing porous media, FlFFF minimizes potential sample interaction with surfaces and fluid shear by utilizing an open channel [16,30,31]. However, sample loss to the bounding membrane remains a consideration in FlFFF [32], and this loss can be minimized by addition of a stabilizing surfactant in the carrier solution [33–37].

The goal of our study was to examine the behavior of different materials associated with processing of Be-ores in simulated lung fluids (SLF) in terms of dissolution, chemical composition, and particle size distribution (PSD) of generated nano-particles. Special attention was focused on behaviors of BeO that contrasted with the other materials. The potential loss of generated nanoparticles to the FlFFF membrane and other FlFFF surfaces was examined quantitatively, as was the potentially incomplete nebulization and ionization of the nanoparticle-containing samples.

Table 1
Summary of the components of the ore samples.

Elements or ores	% in ore		
	Be	Al	SiO_2
BeO	36%	0%	0%
$Be(OH)_2$	20.5%	0%	0%
BERT	0.32%	7.01%	40.36%
BERYL	4.18%	17.80%	63.52%
FRIT	4.23%	17.88%	63.52%
SiO_2	0%	0%	100%

2. Methods and instrumentation

2.1. Sample preparation and sampling procedures

Four types of materials associated with Be processing were examined, including high quality beryl ore (Beryl), heat treated beryl frit from the same lot as the beryl ore (Frit), a bertrandite ore (Bertrandite), and other products of the mill such as beryllium hydroxide ($Be(OH)_2$). Beryllium oxide (BeO) was included as the positive control in this study because it is the classic BeO agent, causing CBD in pure form [38–40], and being omnipresent in dusts and fumes produced by metal processing due to oxidation. Silicon dioxide (SiO_2) was used as a control particle lacking significant Be. Elemental components provided by the Be processing company for each ore material are shown in Table 1. $Be(OH)_2$ and BeO are pure materials which stoichiometrically contain 20.5% and 36.0% Be, respectively. The Beryl, Frit and Bertrandite ores contain Be mass percentages of 4.18%, 4.23%, and 0.32%, respectively; Al mass percentages of 17.8%, 17.9%, and 7.01%, respectively; and Si mass percentages of 63.5%, 63.5%, and 40.4%, respectively. SiO_2 is pure silica dioxide with negligible percentages of Be and Al.

All six of the materials were dry grounded and passed through a 400 mesh screen (38 μm). The particles from each of the ore materials were imaged with SEM. SEM images (Fig. 1) indicate that particles from the different ores (prior to equilibration with SLF) have different shapes and sizes. The Beryl, Bertrandite, and Frit particles show non-uniform size distributions and angular shapes. Beryl ore particles are widely distributed from several hundred nm up to tens of μm. Bertrandite particles range from tens of nm to less than 10 μm in size. Frit particles show glass-like amorphous shapes distributed in size from 1 to 5 μm. $Be(OH)_2$ particles were large (around 200 μm) crystalline aggregates. BeO particles were polydisperse and generally <1 μm in size. SiO_2 particles were polydisperse and generally <500 nm in size.

The six materials described above were equilibrated with synthetic lung fluid (SLF) to simulate the process of particulate equilibration with lung tissue. The SLF consists of common major ions including carbonate and phosphate, as well as citrate, glycine, formaldehyde–methanol solution (concentrations provided in Supporting information) and was purged with pure CO_2 gas for 15 min prior to use. Each material (250 mg) was equilibrated (stirred with Teflon-coated magnets on a shaker table rotating at 100 rpm) with SLF (400 ml) in closed Nalgene wide-mouth polypropylene bottles at two pH values (in parallel bottles) representing the pH value of internal cell fluid (4.5) and external cell fluid (7.2).

The SLF suspensions were sampled (10 ml) on days 0, 2, 8, 16, 32, 64 and 128 of the experiment. Nominally dissolved Be, Al, and Si concentrations in the <450 nm sample fraction (Whatman 0.45 μm syringe filters), were measured by ICP-MS following acidification of the filtered sample (2.4% HNO_3). Size fractions of the particles in the ore suspensions were examined via FFF-ICP-MS for samples from days 0, 4, 8, 32, 49 and 149. Samples for FFF-ICP-MS were filtered (Whatman 5 μm syringe filters) on all sampling days to examine

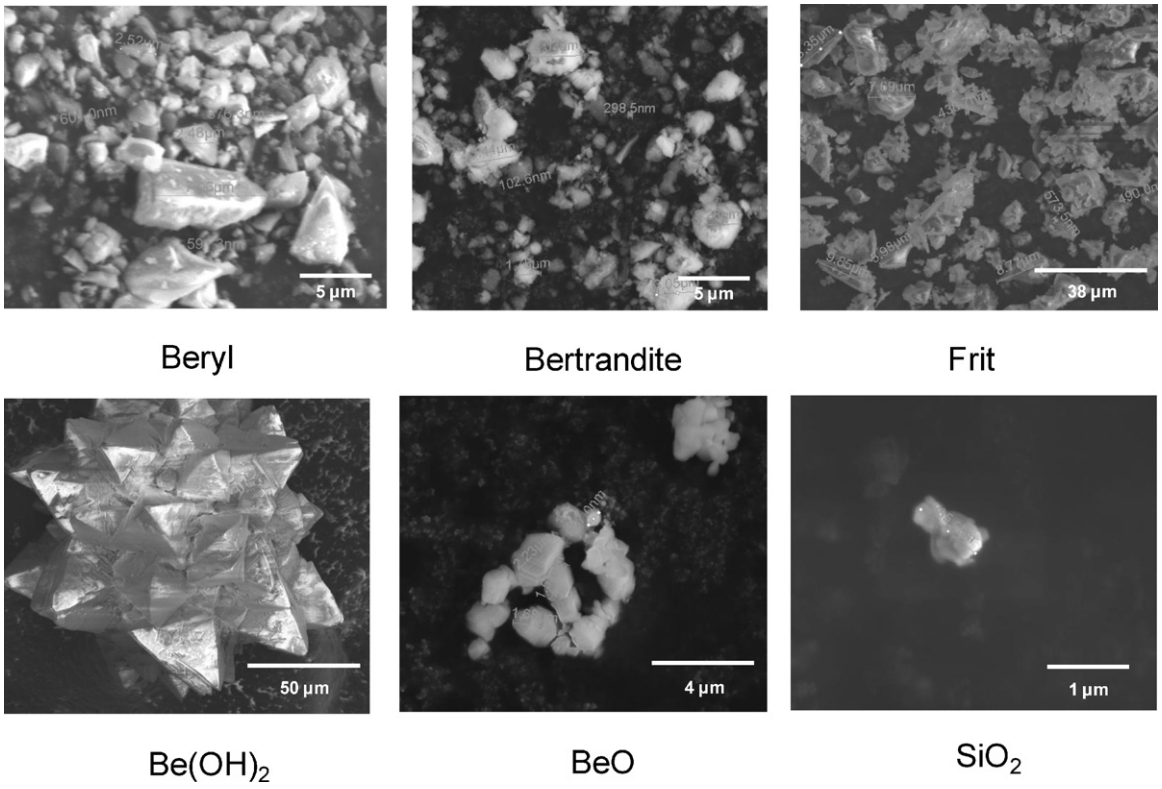

Fig. 1. SEM images of different Be-containing materials examined in this study.

nano-/micro-particulate formation, and were not acidified. Additionally, on day 149 the samples were filtered (Whatman 0.45 μm syringe filter) prior to FFF-ICP-MS analyses for direct comparison to ICP-MS analyses of acidified <450 nm samples.

The pH of each suspension was checked and adjusted (if more than 0.05 pH units off target) using 0.10 M sulfuric acid. On each sampling day the magnetic stirrers were stopped for 30 min to allow settling prior to sampling.

2.2. Flow field-flow fractionation (FIFFF or FFF)

An asymmetric flow field flow fractometer (AF2000, Postnova, Inc., Salt Lake City, UT) was used for particle size separation. The dimensions of the trapezoidal FFF channel were 27.3 cm in length; tapered width from a maximum of 1.7 cm; and an approximate thickness of 315 μm (350 μm spacer). The volume of the channel was approximately 1.5 ml. The injected sample volume was limited to no more than 0.5 ml. The accumulating membrane was regenerated cellulose with a pore size of 10 kDa (Postnova, Inc., Salt Lake City, UT). The injection volume was large due to the low Be content in the samples to be analyzed. The method was particularly tuned for high volume injection: (1) the focus period was set 10 min, so that the injection velocity was moderate; (2) the focusing period was checked with dye to demonstrate it was sufficient for samples to be well focused; (3) the method succeeded in fractionating the same injection volume of diluted standard mixture (10 nm Au, 98 nm, 200 nm and 500 nm latex beads).

Detection was performed using on-line ICP-MS with direct connection from the AF2000 (Agilent 7500ce to the ICP-MS nebulizer. Operating conditions are given in Supporting information. The carrier solution was 0.02% v/v FL-70 with an internal standard (Cs) of known concentration to account for changes in flow and nebulization/ionization efficiency. The pH value of the Fl-70 carrier was 8.93. The ICP-MS counts for Be, Al and Si were normalized to that of the internal standard to account for potential instrumental impacts on measured concentrations.

The operating conditions (Supporting information) for fractionation were optimized using colloidal gold and fluorescent latex beads with sizes 10, 98 and 200 nm for the size range between 10 and 500 nm. The day 149 standards fractogram, and the resulting particle size–retention time function (PS–t), are shown in Fig. 2. The non-linear relationship between particle size and retention time results from the programmed operating condition (Supporting information); with a linearly decreasing cross-flow from an initial value of 1.2 ml/min to 0.3 ml/min within 45 min. The recovery of standards with versus without cross flow was 95%. The calibration curve method was used because: (1) it yielded a straightforward interpretation of results from FFF operating conditions; and (2) did not require a priori knowledge of the diffusivities of the particles resulting from equilibration.

FFF includes three operating stages: focusing stage, elution stage (during which NP are eluted), and a rinsing stage. Elution times (t_i) in the fractograms (corresponding to signal peaks) were converted to sample retention times ($t_{r,i}$) by subtracting the void peak elution time (t_{void}). The PS–t functions used to convert fractograms to size distributions (for each analysis day) are summarized in Table 2.

Elution periods were extended to allow detection of particle sizes potentially exceeding 500 nm. This was done despite having filtered the solution using a 450 nm cutoff filter in order to include

Table 2
Summary of calibration function of FFF for 10–250/500 nm particles on day 4, day 32, day 49, and day 149.

Day	Calibration functions	R-square values
4	$PS = 0.4462t_r^2 + 5.3594t_r$	$R^2 = 1$
32	$PS = 0.1269t_r^2 + 6.0636t_r$	$R^2 = 0.9984$
49	$PS = 0.3984t_r^2 + 6.4945t_r$	$R^2 = 1$
149	$PS = 0.0177t_r^3 - 0.6109t_r^2 + 10.136t_r$	$R^2 = 1$

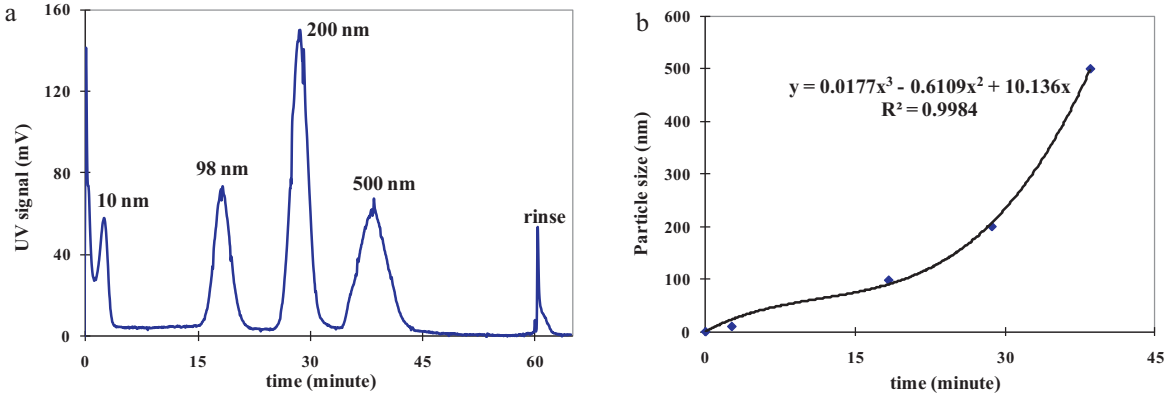

Fig. 2. Calibration of FFF method using mixed standards suspensions (10 nm Au, Latex beads of 98 nm, 200 nm and 500 nm) (a) FFF-UV fractogram and (b) the calibration curve of particle size versus elution time (PS–*t* function).

analysis of irregularly shaped particles that may elute later relative to spherical particles with the same effective hydrodynamic radius. Each filtered sample (500 μl) was injected into the FFF for size analysis in order of low to high concentration (as determined from ICP-MS of acidified <450 nm samples) to minimize residual signal from previous runs.

2.3. Mass integration method from FFF-ICP-MS fractogram

The masses of Be, Al and Si associated with nanoparticles was determined by integrating the area under the ICP-MS fractograms of corresponding elements to determine mass of the element associated with each peak. Masses were converted to concentrations via division by injected volumes. Masses of target elements were integrated from Cs-normalized signals according to Eq. (1) below:

$$\text{Mass}_i(\mu g) = \sum_t \frac{\text{Flow}_{\text{ICPMS}}(\text{ml/min}) \times (CPS_i/CPS_{\text{Cs}}) \times CPS_{\text{Cs,flow=0.4}}}{6 \times 10^4 \times RF_{\text{Cs}}(CPS_{\text{Cs}}/(1\ \ \mu g/L)) \times f_i(CPS_i/CPS_{\text{Cs}})} \quad (1)$$

where $\text{Flow}_{\text{ICP-MS}}$ is the flow rate entering the ICP-MS (0.4 ml/min during the entire sample run); $\text{CPS}_{\text{Cs,flow=0.4}}$ is the ICP-MS signal of internal standard, Cs, in the carrier solution during 0.4 ml min^{-1} flow in the absence of pressure fluctuations that occur during FlFFF fractionation; CPS_{Cs} and CPS_i are the ICP-MS signals from the internal standard and target element during the elution and rinsing steps; RF_{Cs} is the Cs response factor (relating cps to μg/l); and f_i is the ionization efficiency factor (relative to Cs) for each element.

2.4. Be mass balance analysis in FFF-ICP-MS

Two mass fractions in the <450 nm suspensions were defined in this study, according to the cut-off size of the measuring methods: (1) the "truly dissolved" fraction (<3 kDa) that was measured by ultracentrifugal filtration followed by acidification and ICP-MS; (2) the nanoparticle fraction (between 10 nm and 450 nm) that was measured by AF4-ICP-MS. The combined dissolved and nanoparticle mass (<450 nm) was measured by ICP-MS after acidification for comparison.

Losses during FFF were evaluated by comparing elemental mass recoveries from FFF-ICP-MS with and without cross flow. Differences may be attributable to either dissolved elements (<10 kDa) passing through the FFF membrane (by-passing the ICP-MS detector), or to retention on the FFF membrane and other surfaces in the FFF.

Dissolved concentrations of Be, Al, and Si (which would pass through the FFF membrane) were evaluated using <3 kDa centrifugal ultra-filters (Amicon Ultra-4) combined with ICP-MS of acidified filtrate. Samples were placed into the filter, sealed, and centrifuged at 6000 rpm for 45 min. Potential sorption loss of dissolved Be, Al and Si onto the <3 kDa filter membranes was determined to be below 5% in duplicate tests with initial concentrations of 11, 72, and 770 μg/l, respectively in the SLF matrix but with acidification (2.4% HNO_3) to ensure complete dissolution of the target elements.

Assuming that separation of dissolved versus nanoparticle elements was similar for the <3 kDa (Amicon) and <10 kDa (FFF) membranes (assumed on the basis that diameter increases with the cube root of molecular weight), the particulate recovery (R_{FFF}) during fractionation was calculated as:

$$R_{\text{FFF}} = \frac{M_{i,\text{crossflow}}}{M_{i,\text{no crossflow}} - M_{i,<3\ \text{kDa}}} \times 100\% \quad (2)$$

where $\text{Mass}_{\text{crossflow}}$ is the mass of target element integrated from the ICP-MS fractogram with cross flow; $\text{Mass}_{\text{no crossflow}}$ is the mass of target element integrated from the ICP-MS fractogram without cross flow; $C_{<3\ \text{kDa}}$ is the element concentration in the Amicon fil-

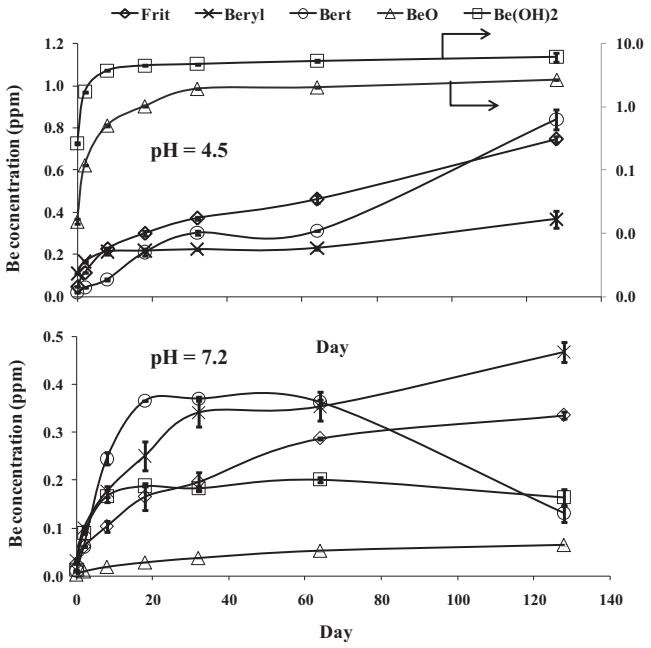

Fig. 3. Concentrations of Be < 450 nm fraction in various ore-SLF suspensions at two pH values: 7.2 (top) and 4.5 (bottom). Samples were collected on day 0, 2, 8, 16, 32, 64 and 128 and measured with bulk ICP-MS. Be concentration of SiO_2 were below the detection limit of ICP-MS. Data are from measurements of duplicate samples with range shown as error bars.

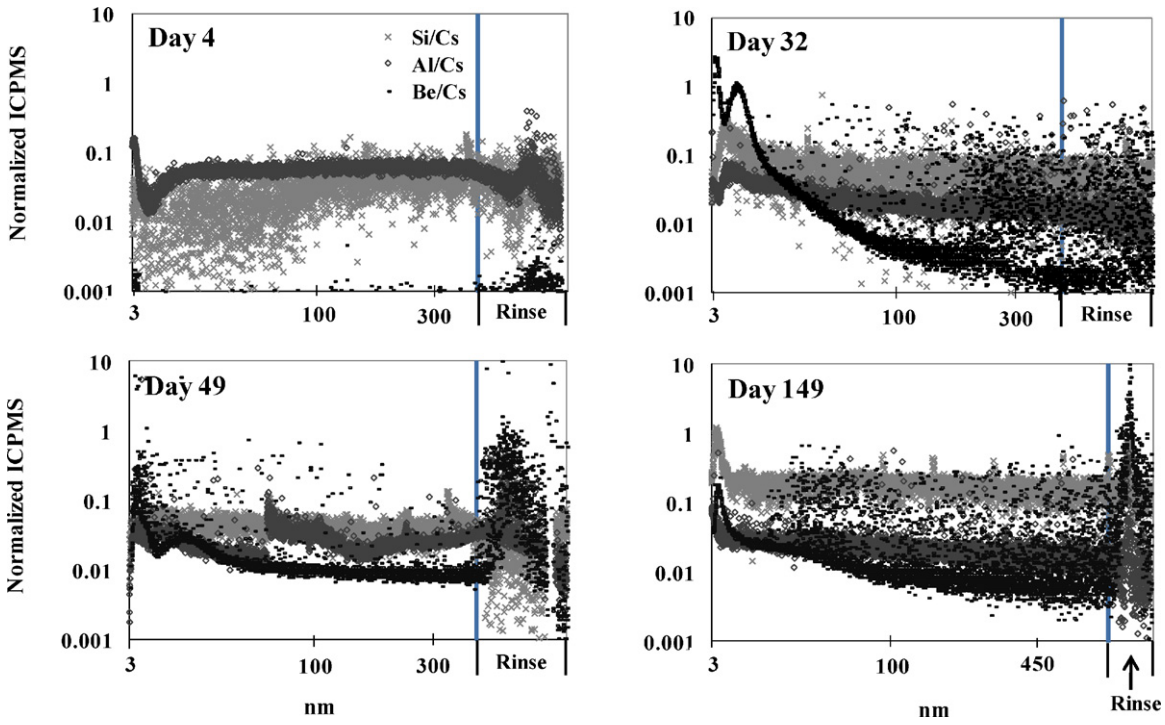

Fig. 4. The ICP-MS fractograms of pH = 4.5 $Be(OH)_2$ suspensions on day 4, day 32, day 49 and day 149. The fractograms are normalized to the internal standard to account for changes in flow and nebulization/ionization efficiencies. The vertical lines represent the start point of rinsing period. The *x*-axis shows size ranges of particles being fractionated.

trate, measured by ICP-MS after acidification of filtrate; and where measured concentration in the <3 kDa filtrate was converted to mass using the sample volume injected into the FFF channel.

Potential losses during ICP-MS analyses include inefficiencies in nebulization and ionization, which are evaluated by comparing integrated masses from FFF-ICP-MS without cross flow ($M_{\text{FFF-ICP-MS no crossflow}}$) to those from ICP-MS of acidified <450 nm samples ($M_{\text{ICP-MS acidified <450 nm}}$) to yield the ICP-MS recovery ($R_{\text{ICP-MS}}$), given by:

$$R_{\text{ICP-MS}} = \frac{M_{\text{FFF-ICP-MS no crossflow}}}{M_{\text{ICP-MS acidified <450 nm}}} \times 100\% \quad (3)$$

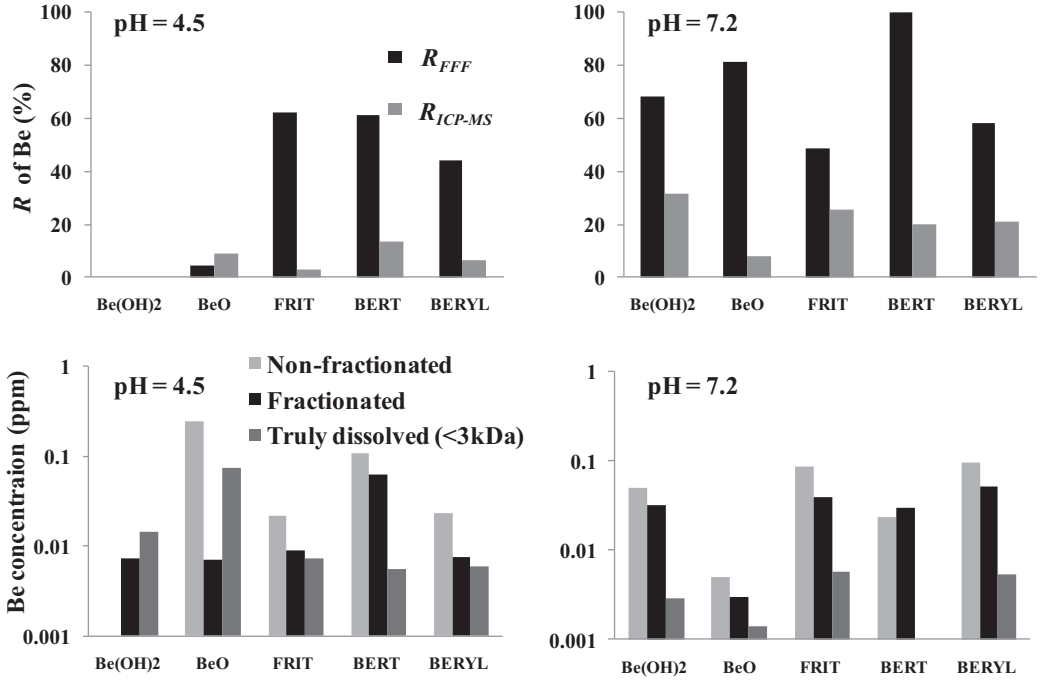

Fig. 5. Be mass recoveries from FlFFF and ICP-MS (top): R_{FFF} shows Be mass percentage of fractionated and non-fractionated (mass recovery in the flow channel); and $R_{\text{ICP-MS}}$ (top) shows the Be mass recovery with versus without acidification (mass recovery due to ionization efficiency). Concentrations (bottom) of Be from Be-containing material suspensions in total (non-fractionated), particulate fraction (FlFFF fractionated) and truly dissolved fraction (<3 kDa centrifugal ultrafiltration). The non-fractionated data of $Be(OH)_2$ suspension were not performed.

where the volume used to obtain $M_{ICP\text{-}MS\ acidified\ <450\,nm}$ from the measured concentration was equal to the sample volume injected into the FFF channel for $M_{FFF\text{-}ICP\text{-}MS\ no\ crossflow}$.

3. Results

3.1. Dissolution behavior of ore suspensions

ICP-MS analyses of acidified equilibrated samples in SLF generally showed rapid increases in Be concentration in the aqueous phase for the first 18 days, with slow or negligible increase from 18 to 128 days (Fig. 3), with the same behavior for Al and Si (Supporting information). Measured Be concentrations from dissolution in SLF (Fig. 3), as well as Al and Si concentrations (Supporting information), showed that dissolution was greater at pH 4.5 relative to 7.2, with maximum Be concentrations ranging from 0.2 to 6.2 ppm at pH 4.5, versus maximum Be concentrations ranging from 0.01 to 0.4 ppm at pH 7.2. $Be(OH)_2$ and BeO showed greater dissolution of Be at pH 4.5; whereas Beryl, Bertrandite, and Frit showed greater Be dissolution at pH 7.2. Bertrandite dissolved much greater Al and Si concentrations relative to the other ores at both pH values (Supporting information).

Dissolution rates were generally greatest during the first 20 days, with a notable exception being the notable increase in Be dissolution from Bertrandite in the pH 4.5 SLF after 60 days (Fig. 3). Also notable is the decrease in aqueous Be (Fig. 3) as well as aqueous Al and Si concentrations (Supporting information) beyond 60 days for Bertrandite in the pH 7.2 SLF, which will be further discussed below. The Be concentrations from SiO_2 in SLF for both pH conditions were below the ICP-MS detection limit.

Be concentrations from BeO and $Be(OH)_2$ suspensions were more than an order of magnitude higher at pH 4.5 relative to pH 7.2

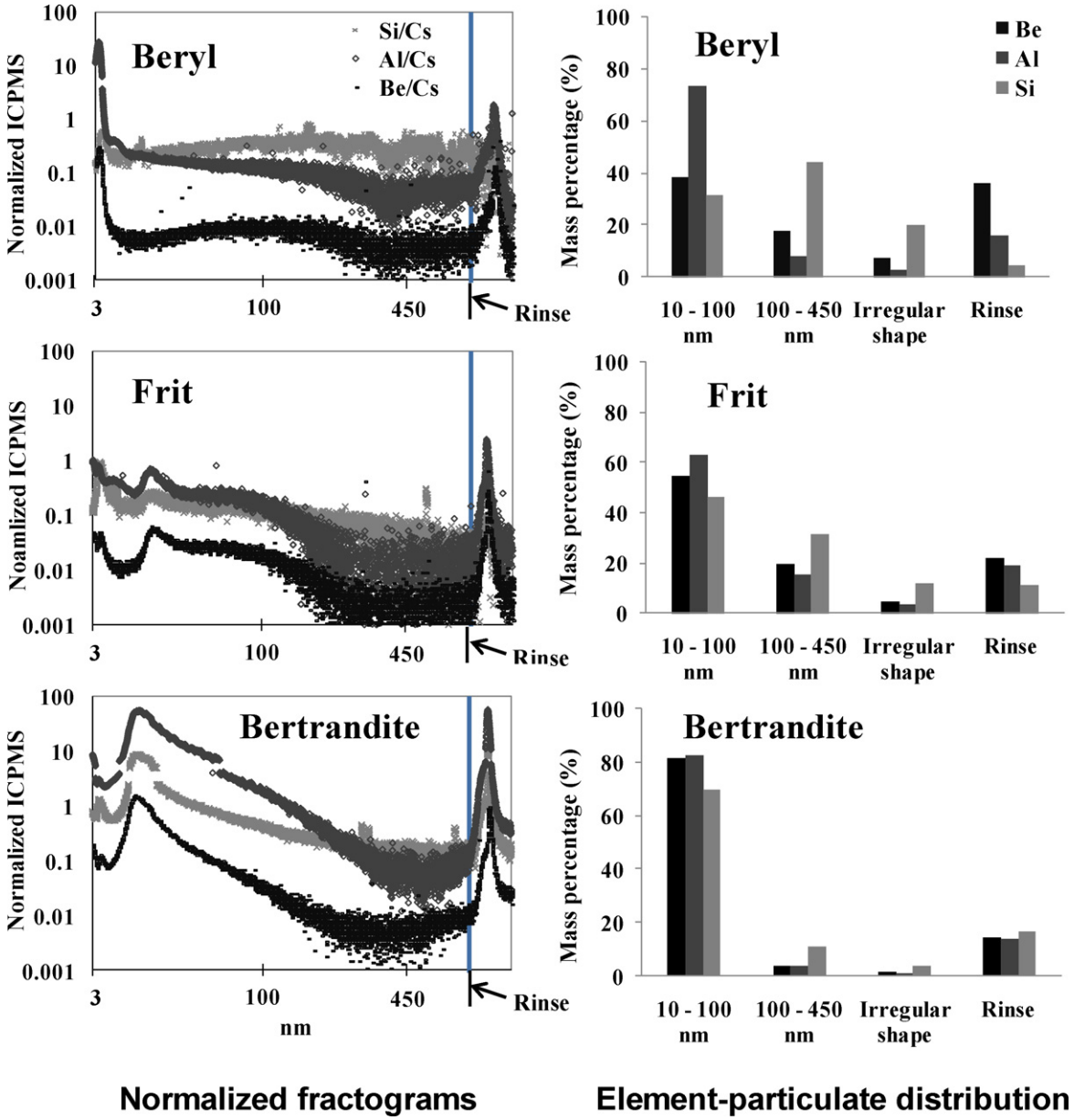

Fig. 6. The normalized ICP-MS fractograms (left) of pH = 4.5 suspensions of Be containing materials: Beryl, Frit, and Bertrandite, normalized to the internal standard to account for changes in flow and nebulization/ionization efficiencies. The vertical lines represent the start point of the rinsing period. Mass %–PSD profiles (right) calculated from the fractograms. The *x*-axis shows size ranges of particles being fractionated: 3–100 nm (lower limit corresponding to 10 kDa accumulating membrane), 100–450 nm (from calibrated FlFFF), and irregular shaped (corresponding to elution following 450 nm-calibrated elution time).

on each sampling day (Fig. 3). The other materials showed comparable Be concentrations at the two pH values.

3.2. Particle formation in ore suspensions

The $Be(OH)_2$ suspension (pH = 4.5) was chosen for examination of time-dependent dissolution and nano-/micro-particles generation since it showed the highest measured Be concentrations among the various ore suspensions during the first 8 days of equilibration (Fig. 3). ICP-MS fractograms of Be, Al and Si for $Be(OH)_2$ suspensions (Fig. 4) indicate that on day 4 no particles containing Be, Al, or Si existed in the <450 nm size range; whereas, Be-, Al- and Si-containing particles were formed by day 32 in the nominal size range of 10–60 nm. The sizes are nominal because the samples were pre-filtered with 5-μm cut-off size filters, allowing any particles that might exist in the size range larger than 1 μm to co-elute during FFF with smaller particles (10–450 nm) under the operating conditions. By day 49, the ICP-MS signal in counts per second (CPS) of Be-associated particles with size of 10 and 60 nm were diminished relative to day 32, and the nominally larger particles corresponding to the rinsing period were relatively increased (Fig. 4), suggesting aggregation of nanoparticles in SLF. This temporal trend continued into day 149.

3.3. Mass balance analysis of Be in FFF-ICP-MS

The sample recovery values (R_{FFF}) of Be for most ore-SLF suspensions were between 50% and 100% (Fig. 5, top), indicating reasonable sample recoveries during fractionation. However, one exception was the pH = 4.5 BeO suspension, where R_{FFF} was less than 10% (Fig. 5). The low R_{FFF} values of Be from the BeO suspension (pH = 4.5) may be linked to (1) its large mass fraction in the truly dissolved form (<3 kDa) (Fig. 5, bottom), which by extension may indicate significant mass in the molecular weight range between 3 kDa and

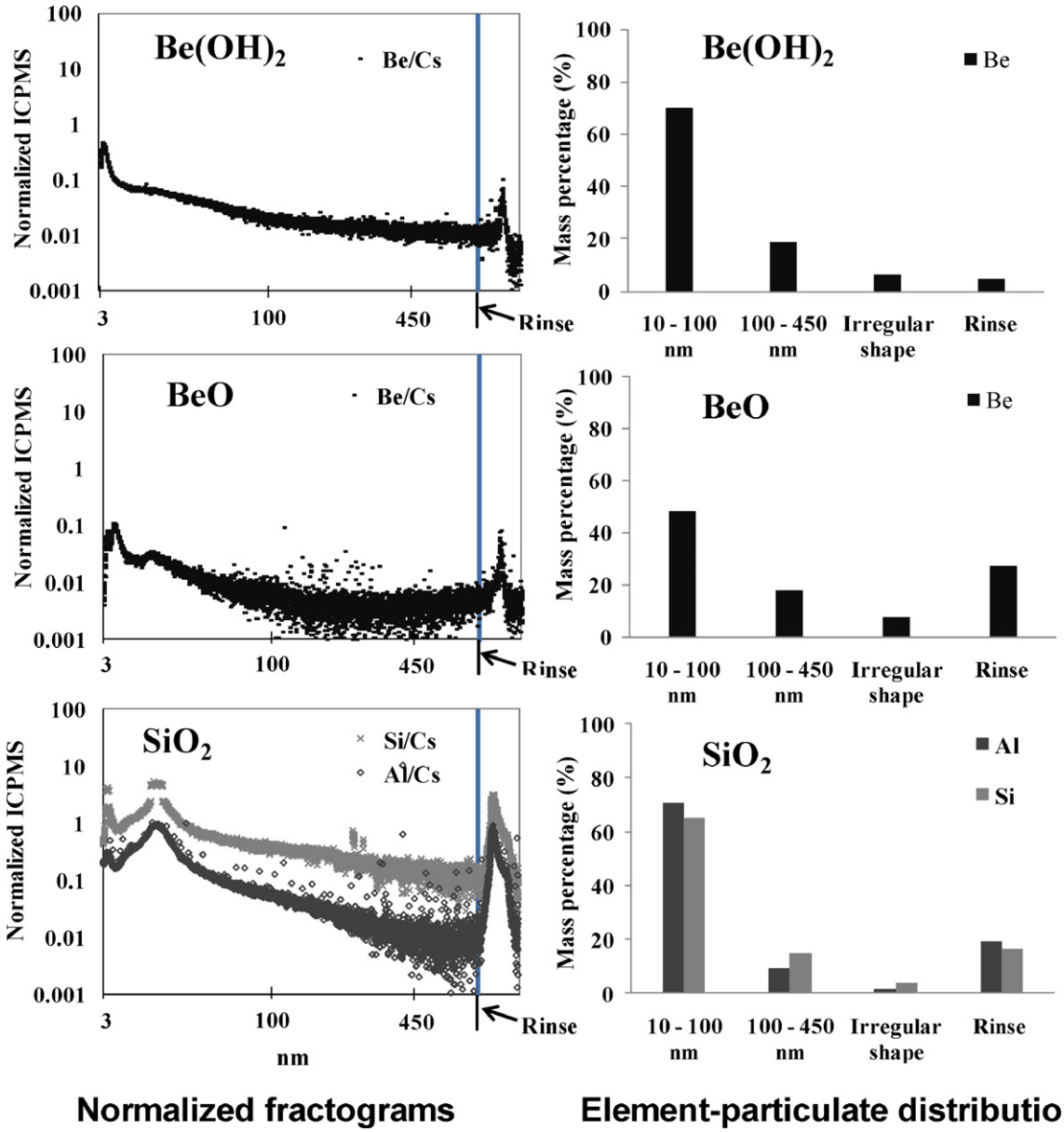

Fig. 7. The normalized ICP-MS fractograms (left) of pH = 4.5 suspensions of Be containing materials: $Be(OH)_2$, BeO, and SiO_2, normalized to the internal standard to account for changes in flow and nebulization/ionization efficiencies. The vertical lines represent the start point of the rinsing period. Mass %–PSD profiles (right) calculated from the fractograms. The *x*-axis shows size ranges of particles being fractionated: 3–100 nm (lower limit corresponding to 10 kDa accumulating membrane), 100–450 nm (from calibrated FlFFF), and irregular shaped (corresponding to elution following 450 nm-calibrated elution time).

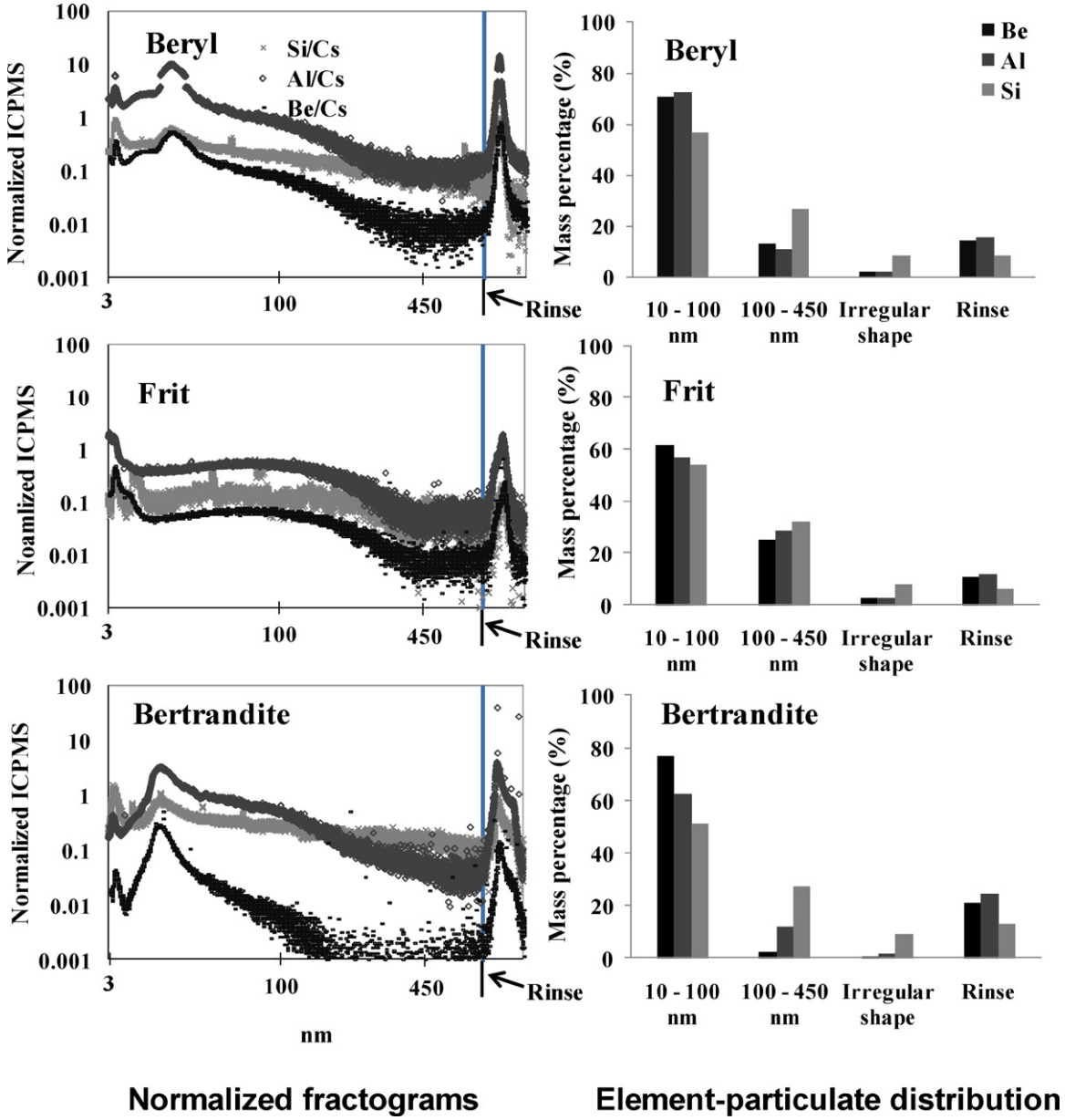

Fig. 8. The normalized ICP-MS fractograms (left) of pH = 7.2 suspensions of Be containing materials: Beryl, Frit, and Bertrandite, normalized to the internal standard to account for changes in flow and nebulization/ionization efficiencies. The vertical lines represent the start point of the rinsing period. Mass %–PSD profiles (right) calculated from the fractograms. The *x*-axis shows size ranges of particles being fractionated: 3–100 nm (lower limit corresponding to 10 kDa accumulating membrane), 100–450 nm (from calibrated FlFFF), and irregular shaped (corresponding to elution following 450 nm-calibrated elution time).

10 kDa membranes, which would be small enough to pass through the FFF membrane, but large enough to not pass through the centrifugal ultrafilter membrane, thereby escaping detection via either method; or (2) dissolution of Be from nanoparticles during FFF-fractionation. Values of R_{FFF} for Al were generally between 50% and 100% for most ore suspensions, except for Bertrandite (pH = 4.5) suspension (<40%) (Supporting information). R_{FFF} values for Si were >100% for most materials (Supporting information), which likely resulted from the high background counts of Si during the ICP-MS analyses; hence we did not focus on Si in our interpretations.

In contrast to R_{FFF}, ICP-MS recovery values ($R_{ICP\text{-}MS}$) of Be, Al and Si were low (5–30%) for the sample suspensions (Fig. 5 and Supporting information). These low values reflect inefficiencies in nebulization and/or ionization of these non-acidified samples. That the R_{FFF} values were between 4% and 30% indicates that losses to/through the FFF membrane were limited during fractionation (aside from the noted exception for BeO at pH 4.5). In contrast, the low $R_{ICP\text{-}MS}$ values raise the possibility that the measured PSDs do not reflect actual PSDs, e.g. particular particle sizes may be preferentially nebulized/ionized. This issue of course represents a major challenge (not usually articulated) for nanoparticle analyses via FFF-ICP-MS. We proceed under the assumption that the observed PSDs are representative of actual PSDs, but future work will further explore this issue.

3.4. Particle size and elemental distribution

Figs. 6–9 show the fractograms and mass distributions of samples after 149 days of equilibration. The results show that the majority of particle-associated Be, Al and Si masses in the <450 nm size range were mainly distributed in the 10–100 nm size range at both pH values. However, BeO showed a more even distribution of

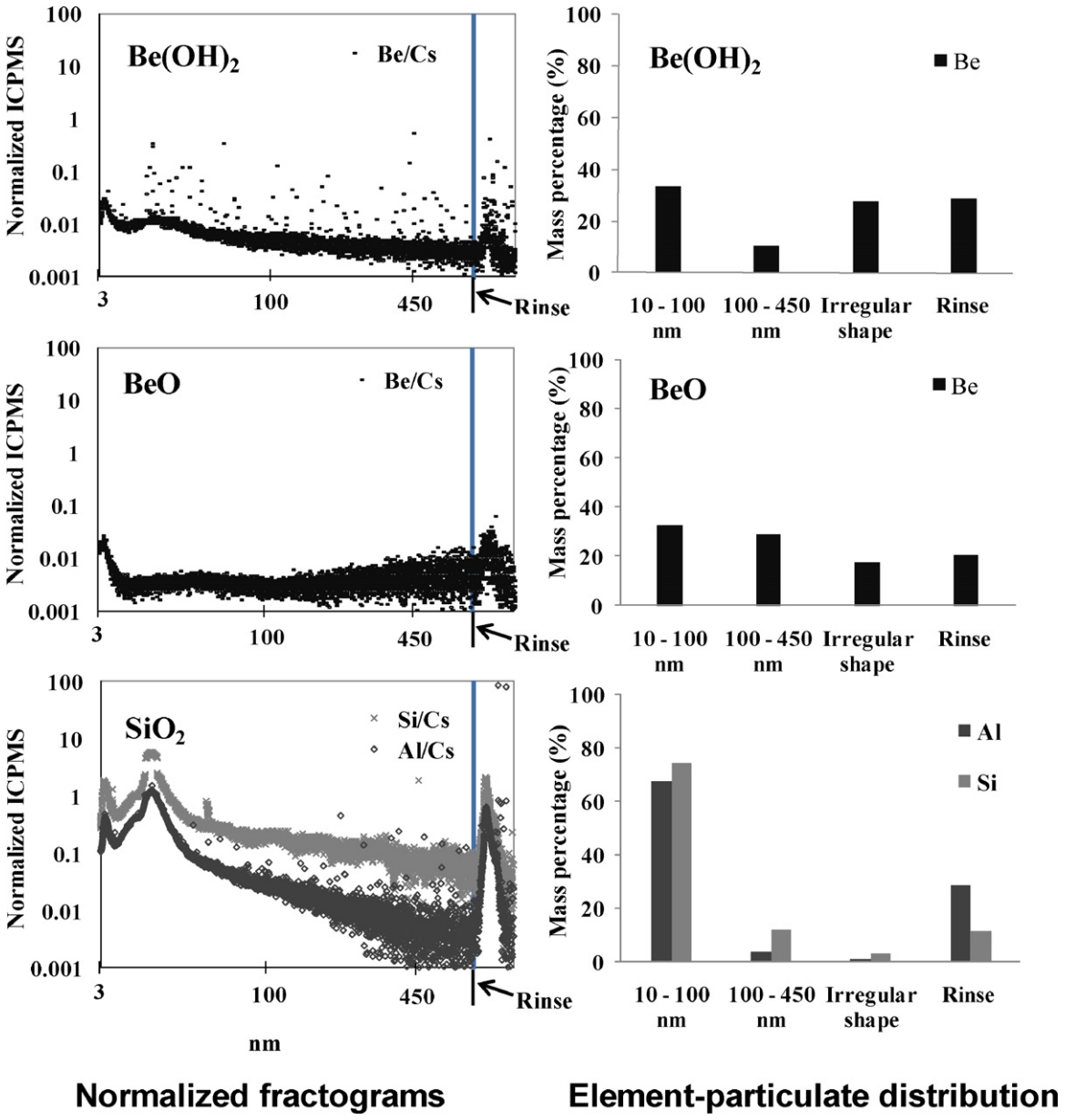

Fig. 9. The normalized ICP-MS fractograms (left) of pH = 7.2 suspensions of Be containing materials: $Be(OH)_2$, BeO, and SiO_2, normalized to the internal standard to account for changes in flow and nebulization/ionization efficiencies. The vertical lines represent the start point of the rinsing period. Mass %–PSD profiles (right) calculated from the fractograms. The *x*-axis shows size ranges of particles being fractionated: 3–100 nm (lower limit corresponding to 10 kDa accumulating membrane), 100–450 nm (from calibrated FlFFF), and irregular shaped (corresponding to elution following 450 nm-calibrated elution time).

mass across the size distribution from 10 to 450 nm relative to the other ores (Figs. 6 and 7 versus Figs. 8 and 9). It should be noted that flow rate varied during ICP-MS analysis; hence higher signals in fractograms during the rinsing step do not necessarily translate to greater integrated masses. In terms of absolute mass, greater particulate mass (<450 nm size fraction) was formed in $Be(OH)_2$, BeO, Bert and SiO_2 suspensions at pH = 4.5 relative to pH = 7.2; while less particulate mass was formed in Beryl and Frit suspensions at pH = 4.5 relative to pH = 7.2 (Fig. 5, bottom). Gaps in some fractograms occurred due to the ICP-MS detector switching to analog mode when the signal exceeded 1E6 CPS (e.g. Al and Si in Bert at pH = 4.5, Al in Beryl and Si in SiO_2 at pH 4.5 and 7.2); however, the resulting mass balance errors were considered negligible since the gaps were small relative to the signals.

Particulate-associated Be concentrations from BeO were more than an order of magnitude higher at pH 4.5 relative to 7.2 (Fig. 5 bottom); whereas particulate-associated Be concentrations from $Be(OH)_2$ were much higher at pH 7.2 relative to pH 4.5 (Fig. 5 bottom). The other materials showed similar particulate Be concentrations at the two pH values. Notably, the truly dissolved (<3 kDa) Be concentrations were much higher for both $Be(OH)_2$ and BeO at pH 4.5 relative to pH 7.2 (Fig. 5, bottom). It should be noted that the very small Be signal in the SiO_2 fractograms at both pH values (Figs. 7 and 9) likely represents Be contamination from previous runs for the other suspensions, since no significant Be masses were detected in SiO_2 via other methods such as ICP-MS without FFF and FFF-ICP-MS without crossflow (Fig. 5, bottom).

4. Discussion

4.1. Dissolution behavior of ore suspensions

The dissolution results from ICP-MS analyses of acidified <450 nm samples demonstrate that dissolution rates for all mate-

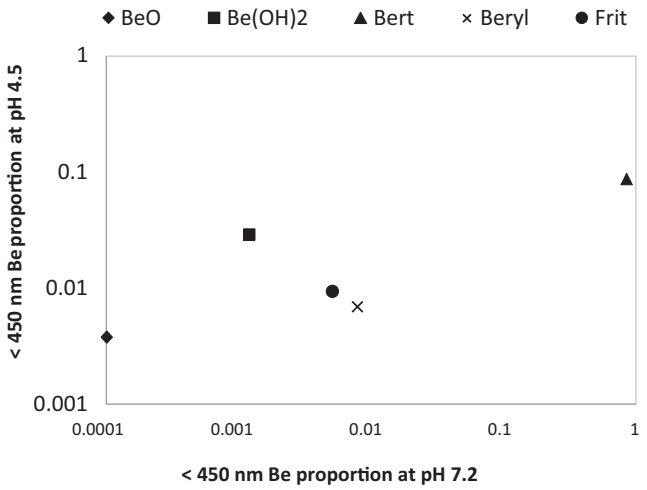

Fig. 10. The <450 nm Be proportion (Be mass in SLF normalized to the initial Be mass content of the ore material) at 18 days of equilibration with SLF at pH = 7.2 (*x*-axis) and pH = 4.5 (*y*-axis). The Be content in SiO_2 was too low to be measured by acidification followed by ICP-MS.

rials were highest during the first 20 days of equilibration and then decreased subsequently. The processes responsible for the observed decline in dissolution rates were not identified, but may include development of dissolution-inhibiting coatings on the surfaces of the materials, e.g. metal oxides or oxyhydroxides, as well as the accumulation of ions in solution beyond the solubility product(s) of corresponding solid phases. The latter possibility is consistent with the generation of nanoparticle phases during equilibration (Figs. 4, 6–9), which in one case led to apparent aggregation and settling removal of elements from solution, as indicated by the decreased solution concentrations of Be, Al, and Si for Bertrandite at pH 7.2 at later times (Fig. 3).

Our simple reactors, in which SLF was equilibrated with Be-containing materials, provide a first-order approximation of dissolution processes in lung tissue. Accumulation of ions in solution in actual biological systems would presumably be limited by interactions with biomolecules; hence the most biologically relevant time period in the dissolution experiments is considered to be that period preceding the observed decrease in dissolution rates, which is likely driven by ion accumulation in solution. Normalizing the dissolution results (Be concentrations in solution) from day 18 of the experiment to the Be content of the parent material yields the proportion of Be dissolving from the parent material, which acts a measure of the persistence of the parent materials (in terms of delivering Be to solution) under the conditions of the experiment. Fig. 10 shows that the proportion of Be in solution was lowest for BeO relative to the other materials under both pH conditions. This was the case despite the Be concentration in pH 4.5 SLF being greater for BeO relative to the other materials except $Be(OH)_2$ (Fig. 3). This observation indicates that among the materials examined, BeO has the highest persistence in both extra- and intra-cellular environments despite producing the second-highest Be concentration in SLF at pH 4.5.

4.2. Particle formation in ore suspensions

As noted above, the accumulation of ions, and subsequent generation of nanoparticles in our system during equilibration times greater than 20 days may not be directly relevant to biological systems. However, it is possible that the observed differences in nanoparticle generation behaviors among the parent materials during later equilibration times provide insight into their respective behaviors that may have relevance to biological systems. In terms of nanoparticle generation, the BeO suspension was distinct from the other suspensions in that the mass distribution was relatively even across this size range (Figs. 7 and 9). It is not clear how this characteristic may relate to the greater inferred toxicity of BeO relative to the other suspensions; however, another distinguishing characteristic of BeO was its relatively low production of nanoparticle Be (and Si and Al) (Figs. 6–9) and its much greater production of truly dissolved Be (<3 kDa) relative to the other materials at pH 4.5 (Fig. 5). The <3 kDa fraction (which is nominally sub-nm in size) may reflect ionic Be; hence, this observation indicates that BeO not only has greater persistence relative to the other materials, but also has a greater propensity to deliver Be in ionic form.

4.3. Mass balance analysis of Be in FFF-ICP-MS

The relatively low $R_{ICP\text{-}MS}$ values (5–30%) obtained are a concern. However, it should be noted that the comparison made was between particles (non-acidified) versus dissolved elements (via acidification) with quantification via integration relative to an internal standard for the former, and via calibration with acidified standards for the latter. The observation indicates that nebulizing and ionizing efficiencies were not equivalent for the acidified standards and the nanoparticle samples. Sample recoveries >90% were reported previously (Table 3) in studies using acidified standards injected in-line downstream of the FFF to obtain concentration–ICP-MS signal (CPS) calibration curve, and use the curve to convert CPS of samples into concentration [24–26,42]. As the calibration curve of acidified standards was used to convert CPS, the assumption was made that the nebulization efficiency of sample particles and dissolved standard was the same. The high recoveries suggest that nebulization/ionization efficiencies were equivalent for the acidified standards and particle samples in those studies. In our study, the integrated mass from the fractogram was compared to the mass from an acidified sample in a matrix different from that in the FlFFF (not containing FL-70 or buffer). Based on the above results, it is possible that our recoveries ($R_{ICP\text{-}MS}$) would be improved if the acidified samples were in a matrix matching that from the FlFFF. To fully remedy the inefficient ionization for analyses of particles, we can potentially follow one of three options: (1) collect discreet size fractions and acidify prior to ICP-MS; (2) use particulate standards in FlFFF; and (3) addition of acid in-line prior to ICP-MS. Option 1 greatly inflates

Table 3
Comparison of the FlFFF sample recovery analyses in existing literature and from this work.

Instrument	Recovery	Material	Cross-flow, ml/min	Quantification method	Reference
FlFFF-UVS	93.1–100%	1430 MW PSS standards	3.8	IS	[36]
FlFFF-UVS	24–98%	DOC in ground water		IS	[41]
FlFFF-ICPMS	>90%	Colloidal metal in natural water	3	LCIS	[24]
FFF-ICPMS	>90%	Metal associated natural colloids	2.96	LCIS	[25]
FlFFF-ICPMS	>90%	Colloids in ground water	4	LCIS	[26]
FlFFF-UVS	95%	Au, Latex standards	0.6–1.2	IS	This study
FlFFF-ICPMS/ ICPMS	5–30%	Be-associated colloids	0.6–1.2	IISNS	This study

Note: IS represents integration of signals; LCIS represents ICP-MS linear calibration of injected standards; IISNS represents integration of internal standard-normalized signals.

the cost of analyses and produces discreet rather than continuous data. Option 2 is impractical because nanoparticle standards for Be simply do not exist that can be *a priori* considered representative of the materials analyzed here. Option 3 requires a design to allow sufficient digestion of sample during the short residence time (<30 s) prior to nebulization. In future studies it will be useful to introduce standards directly in-stream in the FFF-ICP-MS interface in order to achieve equivalent solution conditions for analyses of standards and nanoparticle-containing samples, as well as to attempt quantification via an internal standard to assess internal consistency.

Acknowledgement

This project was supported from a grant from the USDA-CSREES program 2009-35603-05037.

Appendix A. Supplementary data

Supplementary data associated with this article can be found, in the online version, at doi:10.1016/j.chroma.2010.11.070.

References

[1] G.A. Day, A. Dufresne, A.B. Stefaniak, C.R. Schuler, M.L. Stanton, W.E. Miller, M.S. Kent, D.C. Deubner, K. Kreiss, M.D. Hoover, Ann. Occup. Hyg. 51 (2006) 67.
[2] A.K. Madl, K. Unice, J.L. Brown, M.E. Kolanz, M.S. Kent, J. Occup. Environ. Hyg. 4 (2007) 448.
[3] A.B. Stefaniak, M.D. Hoover, G.A. Day, R.M. Dickerson, E.J. Peterson, M.S. Kent, C.R. Schuler, P.N. Breysseb, R.C. Scripsick, J. Environ. Monit. 6 (2004) 523.
[4] R.T. Burnett, J. Brook, T. Dann, C. Delocla, O. Philips, S. Cakmak, Inhal. Toxicol. 12 (2000) 15.
[5] C.P. Arden, R.T. Burnett, M.J. Thun, E.E. Calle, D. Krewski, K. Ito, G.D. Thurston, J. Am. Med. Assoc. 287 (2002) 1132.
[6] E. Norbert, Toxicol. Lett. 149 (2004) 235.
[7] B. Brunekreef, B. Forsberg, Eur. Respir. J. 26 (2005) 309.
[8] W.J. Tracey, J.D. Parker, K.C. Schoendorf, Environ. Health Perspect. 114 (2006) 786.
[9] Z. Antonella, J. Schwartz, Environ. Health Perspect. 117 (2009) 898.
[10] O. Bart, M.L.P. Reynolds, D. Goldberg, A. Hertz, C. Garcia, K.D. Henderson, L. Bernstein, Environ. Health Perspect. 118 (2010) 363.
[11] B. Paul, F.C. Klaessig, T.D. Landry, B. Moudgil, J. Pauluhn, K. Thomas, R. Trottier, S. Wood, Toxicol. Sci. 90 (2006) 23.
[12] D. Ken, L. Tran, L.A. Jimenez, R.D. Duffin, E. Newby, N. Mills, W. MacNee, V. Stone, Part. Fibre. Toxicol. 2 (2005) 1.
[13] C. Buzea, I.I.P. Blandino, K. Robbie, Biointerphase 2 (2007) 17.
[14] J.C. Giddings, Sep. Sci. Technol. 13 (1978) 241.
[15] J.C. Giddings, Sep. Sci. Technol. 19 (1988) 831.
[16] J.C. Giddings, Science 260 (1993) 1456.
[17] S.K. Ratanathanawongs, J.C. Giddings, in: M. Schimpf, K. Caldwell, J.C. Gidding (Eds.), Field-Flow Field Fractionation Handbook, John Wiley & Sons, Inc., New York, 2000.
[18] R. Beckett, Z. Jue, J.C. Giddings, Environ. Sci. Technol. 21 (1987) 289.
[19] R. Beckett, B.T. Hart, in: J. Buffle, V. Leeuwen, H.P. Lewis (Eds.), Environmental Particles, vol. 2, Chelsea, New York, 1993.
[20] M. Baalousha, J.R. Lead, Sci. Total Environ. 386 (2007) 93.
[21] K.G. Wahlund, in: M. Schimpf, K. Caldwell, J.C. Gidding (Eds.), Field-Flow Field Fractionation Handbook, John Wiley & Sons, Inc., New York, 2000.
[22] H. Prestel, L. Schott, R. Niessner, U. Panne, Water Res. 39 (2005) 3541.
[23] P. Dejardin, J. Chromatogr. A 1187 (2008) 209.
[24] M. Hassellov, B. Lyven, R. Beckett, Environ. Sci. Technol. 33 (1999) 4528.
[25] B. Lyven, M. Hassellov, D.R. Turner, C. Haraldsson, K. Andersson, Geochim. Cosmochim. Acta 67 (2003) 3791.
[26] B. Stolpe, M. Hassellov, K. Andersson, D.R. Turner, Anal. Chim. Acta 535 (2005) 109.
[27] M. Baalousha, F.V.D. Kammer, M. Motelica-Heino, M. Baborowski, C. Hofmeister, P. Le Coustumer, Environ. Sci. Technol. 40 (2006) 2156.
[28] M. Bouby, H. Geckeis, F.W. Geyer, Anal. Bioanal. Chem. 392 (2008) 1447.
[29] A. Siripinyanond, R.M. Barnes, Spectrochim. Acta B 57 (2002) 1885.
[30] M. Martin, P.S. Williams, in: C.F. Dondi, G. Guiochon (Eds.), NATO ASI Series, Kluwer Academic, New York, 1992.
[31] J.C. Giddings, Anal. Chem. 67 (1995) 952A.
[32] R. Beckett, J.C. Bigelow, J. Zhang, J.C. Gidding, in: P. MacCarthy, I.H. Suffet (Eds.), Influence of Aquatic Humiv Substances on Fate and Treatment of Pollutants, ACS Advances in Chemistry Series 219, American Chemistry Society, Washington, DC, 1988.
[33] S. Nakatsuka, A.S. Michaels, J. Membr. Sci. 69 (1992) 189.
[34] C.M. Tam, A.Y. Tremblay, J. Membr. Sci. 57 (1991) 271.
[35] M. Balakrishnan, G.P. Agarwal, C.L. Cooney, J. Membr. Sci. 85 (1993) 111.
[36] B. Lyven, M. Hassellov, C. Haraldsson, D.R. Turner, Anal. Chim. Acta 357 (1997) 187.
[37] S. Dubascoux, F. Von Der Kammer, I. Le Hecho, M.P. Gautier, G. Lespes, J. Chromatogr. A 1206 (2008) 160.
[38] K. Kreiss, M.M. Mroz, L.S. Newman, J. Martyny, B. Zhen, Am. J. Ind. Med. 30 (1996) 16.
[39] K. Kreiss, M.M. Mroz, B. Zhen, J. Martyny, L.S. Newman, Am. Rev. Respir. Dis. 148 (1993) 985.
[40] P.K. Henneberger, D. Cumro, D.D. Deubner, M.S. Kent, M. McCawley, K. Kreiss, Int. Arch. Occup. Environ. Health 74 (2001) 167.
[41] F. James, M. Ranville, Jim Hendry, N. Thorsten, Reszat, Qianli Xie, D. Bruce, Honeyman, J. Contam. Hydrol. 91 (2007) 233.
[42] S. Dubascoux, I. Le Hecho, M. Hassellov, F. Von Der kammer, M.P. Gautier, G. Lespes, J. Anal. Atom. Spectrosc. 25 (2010) 613.